

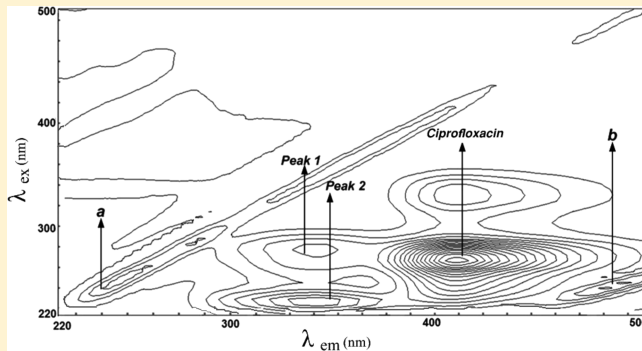
Probing the Interaction of Human Serum Albumin with Ciprofloxacin in the Presence of Silver Nanoparticles of Three Sizes: Multispectroscopic and ζ Potential Investigation

Hedyeh Iranfar,[†] Omid Rajabi,[‡] Roshanak Salari,[‡] and Jamshidkhan Chamani^{†,*}

[†]Department of Biology, Faculty of Sciences, Mashhad Branch, Islamic Azad University, Mashhad, Iran

[‡]Medical Chemistry Department, School of Pharmacy, Mashhad University of Medical Sciences, Mashhad, Iran

ABSTRACT: The binding of ciprofloxacin to human serum albumin (HSA) in the presence and absence of silver nanoparticles of three sizes was investigated for the first time. For this purpose fluorescence spectroscopy, circular dichroism, UV-vis spectroscopy, and ζ potential techniques were employed under physiological conditions. The titration results indicated that ciprofloxacin quenched the fluorescence intensity of HSA through a static mechanism, but in the presence of Ag nanoparticles of sizes I and II there were two different kinds of interaction behavior. Results of circular dichroism indicated that the secondary structure of HSA was modified with increasing ciprofloxacin concentration. A comparison between resonance light scattering of binary and ternary systems allowed us to estimate the effect of silver nanoparticles on the initial formation and aggregation of ciprofloxacin with HSA. The ζ -potential results suggested induced conformational changes on HSA, thus confirming the experimental and theoretical results.



1. INTRODUCTION

Nowadays, nanoparticles (NPs) are gaining much interest in many academic and industrial fields, and reports include plenty of fascinating affects where they are concerned,¹ for example, in biological and medical applications.² This is not only due to the unique optical properties of these NPs, such as size-dependent tunable emission wavelengths and exceptional photochemical stabilities, but also a result of their dimensional similarities with biological molecules.³ With the nanotechnology economy estimated to be worth 1 trillion dollars by 2012, the prevalence of these materials in society will increase. Human exposure to these nanostructured materials is inevitable as they can enter the body through the lungs or other organs via food, drink, or medicine and affect different organs and tissue such as brain, liver, kidney, heart, colon, spleen, bone, blood, etc.⁴

A most prominent nanoparticle is nanosilver. Silver nanoparticles are generally smaller than 100 nm and contain 20–15 000 silver atoms. Silver is a white and brilliant metallic element, positioned 47th in the periodic chart with Ag, meaning “argentum”, as its chemical symbol. At the nanoscale, silver exhibits remarkably unusual physical, chemical, and biological properties,⁵ such as a high molar extinction coefficient, a strong surface, an enhanced Raman scattering effect. It is cheap as well as easy to obtain and detect electrochemically. Consequently, nanosilver is expected to be a new label in bioanalysis.⁶

Ag nanoparticles most notably serve as antimicrobial agents in medical applications. The toxicity of nanosilver may be

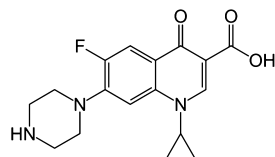
explained by the interaction of nanoparticles with microbes involving silver ion release and cellular internalization of the particles. Size-dependent toxicity of nanosilver supports the mode of action of AgNPs. The nanosilver toxicity is species-specific, and small-sized AgNPs can inhibit nitrifying bacterial growth more than silver ions at identical total silver concentrations.⁷ The biosynthesis of nanoparticles as an emerging highlight of the intersection of nanotechnology and biotechnology has received increasing attention due to a growing need to develop environmentally benign technologies in material synthesis. Silver nanoparticles can be synthesized through an array of methods such as spark discharging, electrochemical reduction, solution irradiation, and cryochemical synthesis. In this work we used electrochemical reduction to prepare Ag nanoparticles of three different sizes.

Fluoroquinolones are a group of broad-spectrum antibacterial agents with a unique mechanism of action and wide clinical use. Their activities result from the inhibition of different kinds of enzymes that control DNA topology and are vital for chromosome function and replication.⁸ Ciprofloxacin [1-cyclopropyl-6-fluoro-1,4-dihydro-4-oxo-7-(piperazinyl)-quinolone-3-carboxylic acid], the structure of which is shown in Scheme 1, is an antibacterial chemotherapeutic from a group of fluoroquinolones.⁹ Its antibacterial spectrum includes Gram-

Received: November 7, 2011

Revised: December 26, 2011

Published: January 6, 2012

Scheme 1. Chemical Structure of Ciprofloxacin

negative and Gram-positive bacteria and its bactericidal activity is rapid. Ciprofloxacin, unlike β -lactam antibiotics, reaches higher levels in bronchial secretions, alveolar macrophages, epithelial lining fluid, and lung parenchyma than those in serum, a property that enhances its therapeutic efficacy in the treatment of pneumonia.¹⁰ Ciprofloxacin is applied through oral or systemic routes, and oral ciprofloxacin treatment is indicated for respiratory infectious diseases such as nosocomial pneumonia.¹¹

Human serum albumin (HSA) is a globular protein consisting of 585 amino acid residues and has three specific binding sites (I, II, and III) for high-affinity binding of drugs. Each of the sites consists of two subdomains (A and B) and is stabilized by 17 disulfide bridges.^{12–14} The two major drug binding sites of HSA, sites I and II, are located in the hydrophobic cavities in subdomains IIA and IIB.¹⁵ HSA plays an important role in the transport, metabolism, and distribution of many endogenous and exogenous ligands such as drugs, fatty acids, hormones, etc., in blood.^{16–18} Also, it is the most abundant protein in blood plasma, accounting for about 60% of the total protein amount, which corresponds to a concentration of 42 g/L. Moreover, it provides about 80% of the osmotic pressure of blood.¹⁹

The concept of drug delivery has emerged from the need for effective management of diseases and can be defined as the delivery of a drug at a rate or at a location determined by a physiological requirement or disease state over a specified period of time.^{20,21} Studies on the binding of drugs to HSA may provide information on structural features that determine the therapeutic effectiveness of drugs, and the topic has become an important research field in life sciences, chemistry, and clinical medicine. Extensive investigations into the interaction between serum albumin and internal compounds or pharmaceutical molecules have been carried out, but the binding of ciprofloxacin with HSA in the presence of Ag nanoparticles has yet to be studied.

The present work aims to report on the affinity of ciprofloxacin to HSA in the presence of Ag nanoparticles of three different sizes as well as their various behaviors in drug delivery. In order to achieve these objectives, spectroscopic techniques and the ζ potential method have been utilized.

2. MATERIALS AND METHODS

2.1. Materials. Human serum albumin (HSA, fatty acid free) and ciprofloxacin, purchased from Sigma Chemical Co., were used without further purification. HSA and ciprofloxacin were dissolved in a potassium phosphate buffer solution (50 mM, pH = 7.4) at concentrations of 4.52×10^{-6} mM and 0.1 mM, respectively, for HSA and ciprofloxacin. The stock solution of HSA was freshly prepared in the buffer. Double-distilled water was used throughout. Three different sizes of silver nanoparticles (i.e., 1.9, 6.5, and 13.7 nm), at 0.5 mM concentration, were prepared by electrochemical reduction.²²

2.2.1. Methods. Procedures. HSA solution (2.0 mL in a 1.0 cm quartz cell) and then titrated by successive additions of

0.1 mM ciprofloxacin in the presence of 0.014 mM Ag nanoparticles to give a final concentration of 1.66×10^{-3} mM. The titration was performed manually and mixed moderately after each injection for 3 min.

2.2.2. Fluorescence and Absorbance Spectroscopy. Fluorescence spectra and intensities were recorded on a FP-6200 spectrophotofluorometer (Jasco, Japan) equipped with a 1-cm quartz cell and a xenon lamp. The widths of both the excitation and emission slits were set to 10 nm. The excitation wavelengths were set to 280 and 295 nm, and the scan speed was 500 nm/min.

UV spectroscopy was performed on a Jasco V-630, linked to a personal computer, with a quartz cuvette with a 1-cm path length. The optical system was based on a split beam with a grating bandwidth of 5 nm, and the light source was a xenon lamp. An appropriate buffer was taken as the blank and subtracted from the experimental spectrum to correct the background fluorescence. All the experiments were repeated at least three times and were performed at room temperature. UV/vis spectra were collected at room temperature on a double-beam UV-630 spectrophotometer (Hitachi Japan) in 1.0-cm quartz cells. The slit width was set to 5 nm, and the wavelength range was 200–500 nm.

2.2.3. Resonance Light Scattering and Synchronous Spectroscopy. Synchronous fluorescence spectra were obtained by simultaneously scanning the excitation and emission monochromators. The synchronous fluorescence spectra showed the Tyr and Trp residues of HSA only when the wavelength interval was 15 and 60 nm, respectively.

Resonance light scattering (RLS) spectra were obtained by simultaneously scanning the excitation and emission wavelengths from 220 to 600 nm with $\Delta\lambda = 0$ nm. RLS data has been known to provide information on the aggregation of small molecules as well as on the long-range assembly of drugs on biological templates.

2.2.4. Circular Dichroism Spectroscopy. Circular dichroism (CD) spectra were recorded with a Jasco J-815 automatic recording spectropolarimeter (Jasco Spectroscopic Co., Japan), with a quartz cell with a path length of 1 mm. The concentration of HSA was 0.01% (w/v). Spectra were collected with scan speed of 100 nm/min, bandwidth of 1 nm, measuring range of 190–250 nm, and standard sensitivity. All of the experiments were performed at room temperature. Dry nitrogen gas was utilized to purge the testing environment before and during the measurements.

The samples for CD analysis were prepared with a fixed concentration of HSA and varying drug concentrations in the presence of silver nanoparticles of three sizes, resulting in equal volumes. The instrument was calibrated with ammonium d-10-camphorsulfuric acid. The induced ellipticity, expressed in degrees, was obtained for the drug–HSA mixtures by subtracting the ellipticity of the drug at the same wavelength. The results were expressed as the mean residue ellipticity (θ), defined as $[\theta] = 100\theta_{\text{obsd}}/\text{LC}$, where θ_{obsd} is the observed ellipticity in degrees, C is the concentration of the residue in moles per cubic centimeter, and L is the length of the light path in the cell. All pH measurements were performed with a Metrohm digital pH-meter (Metrohm, Germany).

2.2.5. Zeta Potential Measurements. A surface potential can be obtained when the charge of colloidal particles accumulates at their surface. This potential is a significant factor for determining the dimension of charged-based colloidal

interactions of a particle, most often electrostatic, with other like-charged particles.

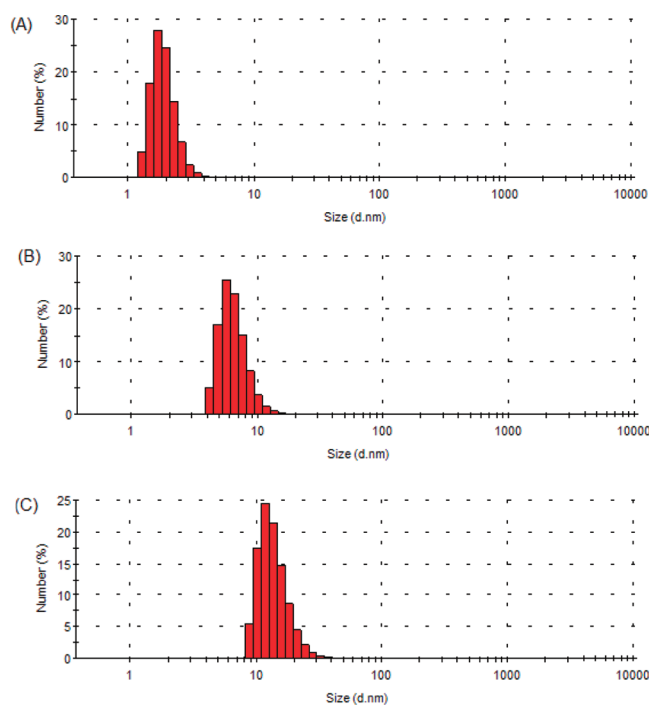
The ζ potential was determined by laser Doppler electrophoresis, and the measurements were performed on a Zeta Sizer Non series-ZS (Malvern Instruments, Malvern, U.K.) at 298 K for drugs and protein. The initial volume of HSA was 1000 μL , into which injections of different volumes of the stock drug solution were added.

2.2.6. Electrochemical Reduction Method. Chemical reduction is the most frequently used method for preparation of silver nanoparticles (AgNPs) as colloidal dispersions in water or organic solvents. The reduction of silver ions (Ag^+) in aqueous solution generally yields colloidal silver with particle diameters of several nanometers. Initially, the reduction of various complexes with Ag^+ ions leads to the formation of silver atoms, which is followed by agglomeration into oligomeric clusters. These clusters eventually give rise to the formation of colloidal Ag particles.

Controlled synthesis of AgNPs is based on a two-step reduction process. In this technique, a strong reducing agent is used to produce small Ag particles, which are enlarged in a secondary step by further reduction with a weaker reducing agent. Different studies have reported on the enlargement of particles in the secondary step from about 20–45 nm to 120–170 nm. Moreover, the initial sol is not reproducible and specialized equipment is required. The synthesis of nanoparticles by chemical reduction methods is therefore often performed in the presence of stabilizers in order to prevent unwanted agglomeration of the colloids.²²

2.2.7. Transmission Electron Microscopy. In order to study the morphology of silver nanoparticles and confirm their aggregation, we analyzed their sizes. Scheme 2 shows size

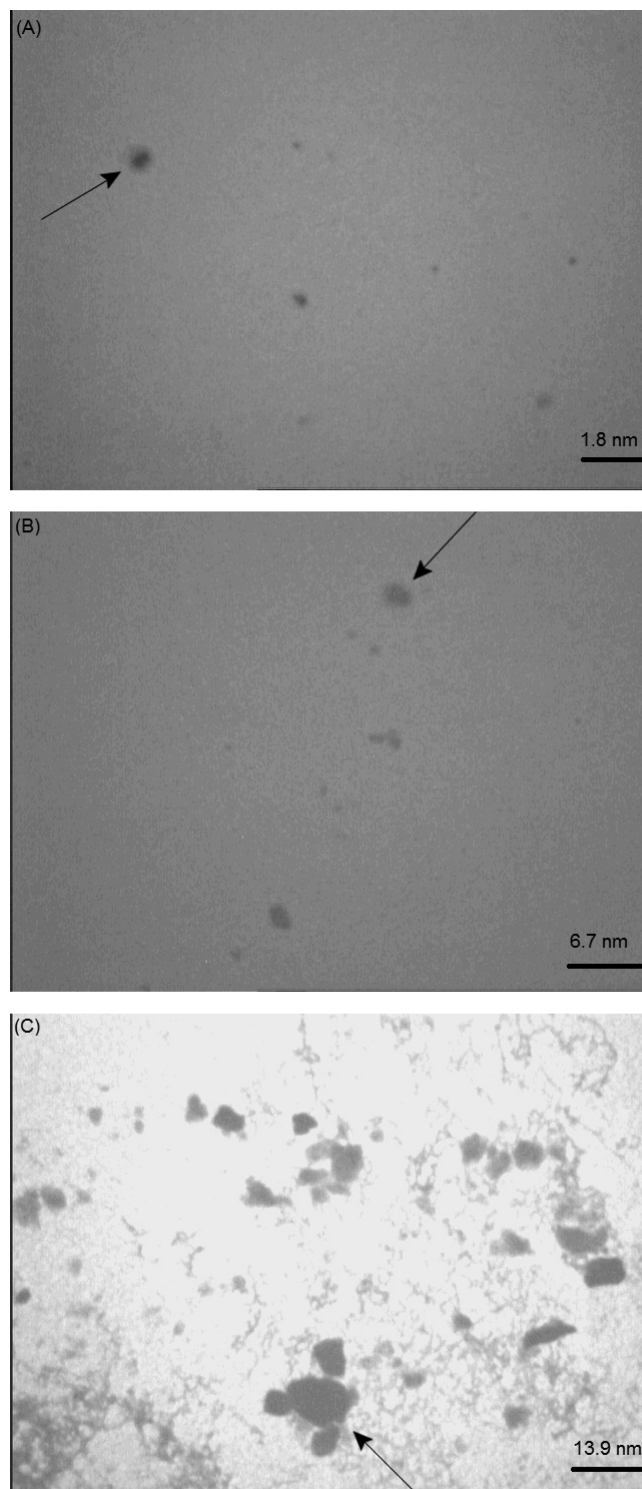
Scheme 2. Size Distribution Curves by Number Percentage for Silver Nanoparticles^a



^aThree different sizes of silver nanoparticles are shown: (A) size I, (B) size II, and (C) size III.

distribution curves and Scheme 3 shows TEM micrographs of the different-sized silver nanoparticles. The shape of the

Scheme 3. Morphologies of Silver Nanoparticles by TEM^a



^aAggregated nanoparticles are marked by arrows: (A) size I, (B) size II, and (C) size III.

particles was globular, but at high concentrations they aggregated and their size was increased. By comparing TEM images of the three silver nanoparticle types, it was concluded that with larger size, their aggregation increased. Moreover, it

was possible to estimate the size of the silver nanoparticles from the TEM images.

3. RESULTS AND DISCUSSION

3.1. Fluorescence Quenching Mechanism. The fluorescence method is an important tool for investigating the interaction between small probe molecules and proteins.²³ Most proteins can emit intrinsic fluorescence after absorbing ultraviolet light, provided that there are residues such as tryptophan (Trp), tyrosine (Tyr), and phenylalanine (Phe) in their molecular interaction. This is called fluorescence quenching. The degree of fluorescence quenching suggests changes in the protein structure and microenvironment around the above-mentioned residues. For macromolecules, fluorescence measurements can give information on the molecular level of binding of small molecular substances to the protein, such as the binding mechanism, binding mode, binding constants, binding studies, intermolecular distances, etc.²⁴

A valuable feature of intrinsic fluorescence of a protein is the high sensitivity of Trp to its local environment. Changes in emission spectra of Trp are common in response to the protein's conformational transition, subunit association, substrate binding, or denaturation.²⁵ Protein fluorescence is generally excited at the absorption maximum near 280 nm or at longer wavelengths. The absorption of proteins at 280 nm is due to both Tyr and Trp residues, whereas at wavelengths longer than 295 nm, the absorption is primarily due to Trp. Trp fluorescence can thus be selectively excited at 295–305 nm.

Tyr is often regarded as a rather simple fluorophore. However, under some circumstances, Tyr can also display complex spectral properties. Tyr emission is observable in certain proteins, but it appears that excited-state ionization is not a major decay pathway for Tyr in proteins. Thus, the intrinsic fluorescence of proteins can provide considerable information about their structure and dynamics, and it is often considered during the study of protein folding and association reactions.²⁴

The fluorescence spectra of HSA with different concentrations of ciprofloxacin at $\lambda_{\text{ex}} = 280$ and 295 nm are shown in Figure 1. Ciprofloxacin exhibited native fluorescence at 380–470 nm. The spectra indicate that, with increasing ciprofloxacin concentrations, the fluorescence intensity of HSA was decreased and the ciprofloxacin peak increased in a regular manner (fluorescence spectra of HSA and ciprofloxacin are in two different regions and do not overlap). Moreover, the blue shift in the fluorescence spectra corresponded to decreased polarity of the microenvironment after binding, which indicates that the chromophore of the protein was brought to more hydrophobic surroundings. Also, an isosbestic point can be seen, at which HSA–ciprofloxacin has the same fluorescence intensity at about 378 nm. The isosbestic point is indicative of equilibrium between bound and free forms of the ligand. Fluorescence spectra of (HSA-AgI)–ciprofloxacin, (HSA-AgII)–ciprofloxacin, and (HSA-AgIII)–ciprofloxacin (data not shown) pointed toward the same results. All of these spectral changes suggest the formation of an HSA–ciprofloxacin complex in both the presence and absence of silver nanoparticles of different sizes.

3.2. Stern–Volmer Quenching Studies. The fluorescence quenching of a protein by small molecules can be static

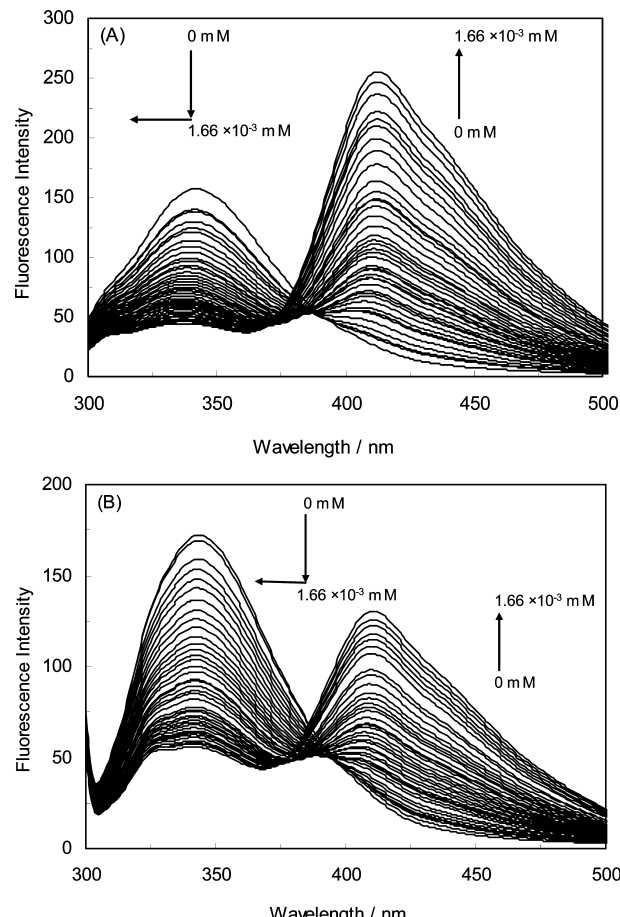


Figure 1. Emission fluorescence spectra of HSA at varying concentrations of ciprofloxacin at (A) $\lambda_{\text{ex}} = 280$ nm and (B) $\lambda_{\text{ex}} = 295$ nm. $T = 298$ K, pH 7.4, $C_{\text{HSA}} = 4.52 \times 10^{-6}$ mM.

and/or dynamic in nature.²⁶ The Stern–Volmer equation is often applied to describe the fluorescence quenching:

$$F_0/F = 1 + k_q \tau_0 [Q] = 1 + K_{\text{SV}} [Q] \quad (1)$$

where F_0 and F are the fluorescence intensity before and after addition of the quencher, respectively; K_{SV} is the Stern–Volmer dynamic quenching constant, which represents a direct measure of the quenching efficiency; k_q is the quenching rate constant of the biomolecule; τ_0 is the average lifetime of the biomolecule; and $[Q]$ is the concentration of the quencher.²⁶

The value of k_q is deduced by the following equation:

$$K_{\text{SV}} = k_q \tau_0 \quad (2)$$

where τ_0 is 10^{-8} s and K_{SV} is the slope of linear regressions of the curve F_0/F versus $[Q]$. Fluorescence quenching behavior of the protein and Stern–Volmer analysis of the relative fluorescence intensity (F_0/F) as a function of the quencher concentration $[Q]$ were employed to elucidate the quenching mechanism and rates (Figure 2). Tables 1 and 2 list binding constants obtained from the Stern–Volmer method, and as can be seen, all the k_q values from the protein quenching procedures were greater than k_q of the biopolymer ($2.0 \times 10^{10} \text{ M}^{-1} \cdot \text{s}^{-1}$). This indicated that the quenching was not initiated from dynamic collision but from complex formation.

According to Tables 1 and 2, in the (HSA-AgI)–ciprofloxacin and (HSA-AgII)–ciprofloxacin systems there were two linear Stern–Volmer equations and two k_q values, obtained in the

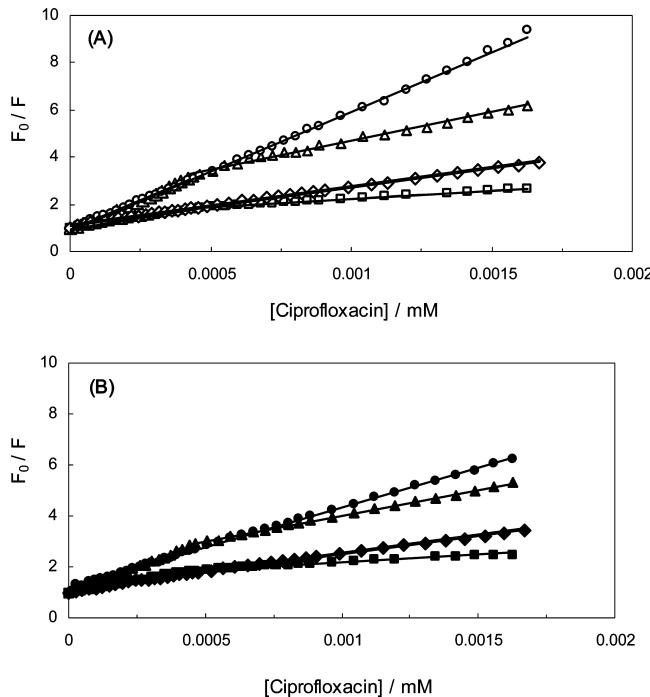


Figure 2. Stern–Volmer plots for fluorescence quenching of HSA at (A) $\lambda_{\text{ex}} = 280 \text{ nm}$ and (B) $\lambda_{\text{ex}} = 295 \text{ nm}$: (◊, ◆) HSA–ciprofloxacin; (□, ■) (HSA–AgI)–ciprofloxacin; (△, ▲) (HSA–AgII)–ciprofloxacin; (○, ●) (HSA–AgIII)–ciprofloxacin.

presence of nanosilver sizes I and II. There were thus two sets of binding sites with two different interaction behaviors, while in the (HSA–ciprofloxacin) and (HSA–AgIII)–ciprofloxacin systems there was only one binding site. This demonstrates that silver nanoparticles of different sizes had different behaviors when inducing HSA–ciprofloxacin complexes. Moreover, the K_{SV} values increased with increasing size of the silver nanoparticles, indicating that the affinity of ciprofloxacin to HSA was greater in the presence of larger silver nanoparticles as opposed to smaller ones.

For static quenching, the Stern–Volmer quenching constant can be interpreted as an association constant or binding constant (K) since static quenching arises from the formation of a complex between fluorophores and a quencher. Hence, the binding constant (K) was calculated by the method given in the following section. It was found that there existed various K_{SV} and k_q values in the presence of different sizes of Ag nanoparticles, which indicated that a change in the Ag nanoparticle size induced different behaviors.

For a static quenching procedure, the data were analyzed according to the modified Stern–Volmer equation:

$$\frac{F_0}{\Delta F} = \frac{1}{f_a K_a} \frac{1}{[Q]} + \frac{1}{f_a} \quad (3)$$

Table 1. Stern–Volmer Quenching Constants at $\lambda_{\text{ex}} = 280 \text{ nm}$ for Interaction of Ciprofloxacin with HSA in the Absence and Presence of Silver Nanoparticles

system	$K_{\text{SV1}} \times 10^{-6}/\text{M}^{-1}$	$K_{\text{SV2}} \times 10^{-6}/\text{M}^{-1}$	$k_{q1} \times 10^{-14}/\text{M}^{-1}\cdot\text{s}^{-1}$	$k_{q2} \times 10^{-14}/\text{M}^{-1}\cdot\text{s}^{-1}$	R_1	R_2
HSA–ciprofloxacin	1.607 ± 0.023		1.607 ± 0.023			0.998
(HSA–AgI)–ciprofloxacin	1.939 ± 0.026	0.691 ± 0.026	1.939 ± 0.026	6.91 ± 0.026	0.997	0.996
(HSA–AgII)–ciprofloxacin	5.055 ± 0.031	2.454 ± 0.031	5.055 ± 0.031	2.454 ± 0.031	0.993	0.992
(HSA–AgIII)–ciprofloxacin	5.05 ± 0.022		5.05 ± 0.022			0.998

In the present case, ΔF is the difference in fluorescence in the absence and presence of the quencher at concentration $[Q]$, f_a is the fraction of accessible fluorophore, and K_a is the effective quenching constant for the accessible fluorophores, which is analogous to an associative binding constant for the quencher–acceptor system.

The dependence of $F_0/\Delta F$ on the reciprocal value of the quencher concentration $[Q]^{-1}$ was linear, with the slope equaling the value of $(f_a K_a)^{-1}$. The value f_a^{-1} was fixed on the ordinate, and the constant K_a was a quotient of the ordinate f_a^{-1} and the slope $(f_a K_a)^{-1}$. The f_a values at $\lambda_{\text{ex}} = 280$ and 295 nm of HSA–ciprofloxacin in the absence and presence of different sized nanosilver are listed in Tables 3 and 4.

As can be seen, the presence of silver nanoparticles affected the f_a values. An f value equal to 1 indicated that all the Trp residues were accessible to the quencher. Consequently, a change in the value of f caused the fraction of fluorescent components that were accessible to the quencher to become altered.²⁷ In this case, for the HSA–ciprofloxacin complex, about 83.4% of Trp and Tyr were accessible to ciprofloxacin. By increasing the size of the silver nanoparticles in the ternary systems, the value of f_a reached almost 1 for the (HSA–AgIII)–ciprofloxacin system. Thus, in this case, almost 100% of the Trp and Tyr became accessible to ciprofloxacin.

Figure 3 shows quenching curves for the HSA–ciprofloxacin complex in the presence and absence of silver nanoparticles at $\lambda_{\text{ex}} = 280 \text{ nm}$ (Figure 3A) and $\lambda_{\text{ex}} = 295 \text{ nm}$ (Figure 3B). Since an overlap occurred between the two excitation wavelengths (data not shown), it could be concluded that ciprofloxacin bound solely to the Trp residues of HSA.

3.3. Analysis of the Binding Constant. For the static quenching interaction, if it is assumed that there are similar and independent binding sites in the biomolecule, the relationship between the fluorescence intensity and the quenching medium can be deduced from the following formula:^{28,29}



Here, B is the biomolecule with a fluorophore, Q is the quencher molecule, and $Q_n B$ is the quenched biomolecule complex whose resultant constant is K_a calculated according to

$$K_a = [Q_n B]/[Q]^n[B] \quad (5)$$

If the overall amount of biomolecule (bound or unbound with the quenchable molecule) is B_0 , then $[B_0] = [Q_n B] + [B]$, where $[B]$ is the concentration of unbound biomolecule. The relationship between fluorescence intensity and the unbound biomolecule then becomes

$$[B]/[B_0] = F/F_0 \quad (6a)$$

or in other words

$$\log [(F_0/F)/F] = \log K_a + n \log [Q] \quad (6b)$$

Table 2. Stern–Volmer Quenching Constants at $\lambda_{\text{ex}} = 295 \text{ nm}$ for Interaction of Ciprofloxacin with HSA in the Absence and Presence of Silver Nanoparticles

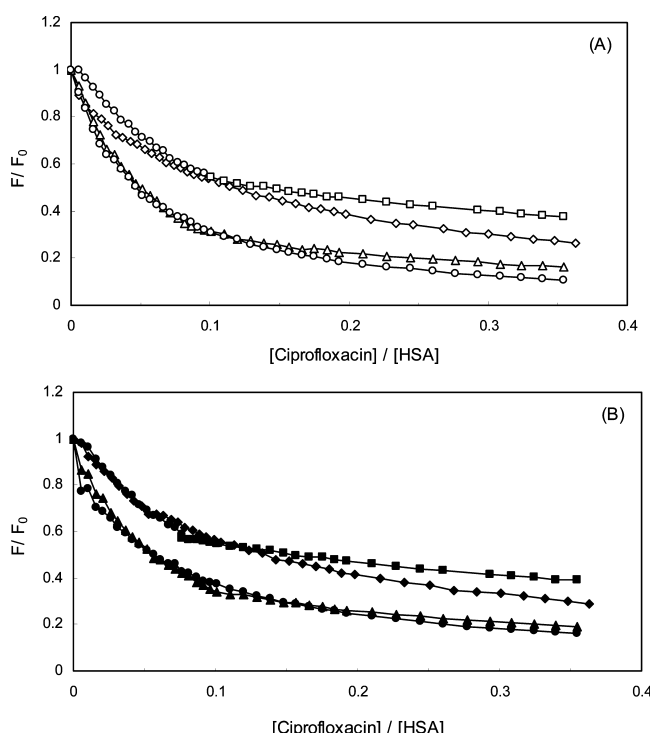
system	$K_{\text{sv1}} \times 10^{-6}/\text{M}^{-1}$	$K_{\text{sv2}} \times 10^{-6}/\text{M}^{-1}$	$k_{\text{q1}} \times 10^{-14}/\text{M}^{-1}\cdot\text{s}^{-1}$	$k_{\text{q2}} \times 10^{-14}/\text{M}^{-1}\cdot\text{s}^{-1}$	R_1	R_2
HSA–ciprofloxacin	1.437 ± 0.021		1.437 ± 0.021		0.996	
(HSA-AgI)–ciprofloxacin	2.045 ± 0.024	0.651 ± 0.024	2.045 ± 0.024	0.651 ± 0.024	0.996	0.998
(HSA-AgII)–ciprofloxacin	4.066 ± 0.022	2.02 ± 0.022	4.066 ± 0.022	2.02 ± 0.022	0.995	0.998
(HSA-AgIII)–ciprofloxacin	3.131 ± 0.021		3.131 ± 0.021		0.998	

Table 3. Fractions of Accessible Protein at $\lambda_{\text{ex}} = 280 \text{ nm}$

system	f_{a1}	f_{a2}	R_1	R_2
HSA–ciprofloxacin	0.834		0.985	
(HSA-AgI)–ciprofloxacin	0.715	1.863	0.988	0.993
(HSA-AgII)–ciprofloxacin	0.905	0.834	0.995	0.998
(HSA-AgIII)–ciprofloxacin	1.011		0.997	

Table 4. Fractions of Accessible Protein at $\lambda_{\text{ex}} = 295 \text{ nm}$

system	f_{a1}	f_{a2}	R_1	R_2
HSA–ciprofloxacin	1.006		0.997	
(HSA-AgI)–ciprofloxacin	0.672	0.914	0.972	0.992
(HSA-AgII)–ciprofloxacin	0.883	0.977	0.985	0.984
(HSA-AgIII)–ciprofloxacin	0.904		0.99	

**Figure 3.** Quenching curves of HSA by ciprofloxacin at (A) $\lambda_{\text{ex}} = 280 \text{ nm}$ and (B) $\lambda_{\text{ex}} = 295 \text{ nm}$: (\diamond , \blacklozenge) HSA–ciprofloxacin; (\square , \blacksquare) (HSA-AgI)–ciprofloxacin; (\triangle , \blacktriangle) (HSA-AgII)–ciprofloxacin; (\circ , \bullet) (HSA-AgIII)–ciprofloxacin.

where K_a is the binding constant and n is the number of binding sites.²⁴

The values of K_a and n are listed in Tables 5 and 6. As can be seen, the interaction between HSA and ciprofloxacin in the presence of AgI and AgII is different from AgIII. In the presence of AgI and AgII, there are two different binding sites with various affinities that depend on the size of nanosilver. It is clearly shown that the interaction between HSA and ciprofloxacin in the presence of nanosilvers with different sizes have two different behaviors; therefore, nanosilvers with different sizes have different applications in protein solution that can be related to their different hydration layers. K_a is a measure of the affinity of the protein to the drugs, suggesting that the K_a value for HSA–ciprofloxacin increased in the presence of silver nanoparticles at $\lambda_{\text{ex}} = 280 \text{ nm}$. On the contrary, the K_a value for HSA–ciprofloxacin increased at $\lambda_{\text{ex}} = 295 \text{ nm}$ when nanosilver of size I and II was added but decreased in the presence of size III. These results led to the conclusion that the interaction between ciprofloxacin and HSA changed after the addition of silver nanoparticles to the HSA–ciprofloxacin complex. Consequently, the silver nanoparticles caused a stronger complex to be established. The interaction behavior of HSA–ciprofloxacin changed with the presence of the silver nanoparticles in the ternary system. Also, the affinity binding for the binary and ternary systems at $\lambda_{\text{ex}} = 280 \text{ nm}$ was higher than at $\lambda_{\text{ex}} = 295 \text{ nm}$, because at $\lambda_{\text{ex}} = 280 \text{ nm}$ both Tyr and Trp were excited, whereas at $\lambda_{\text{ex}} = 295 \text{ nm}$ only Trp was excited.

3.4. Characteristics of Synchronous Fluorescence Spectra.

Synchronous fluorescence spectroscopy, introduced by Lloyd and Evett,³⁰ has been used to characterize complex mixtures, providing fingerprints of intricate samples. Synchronous fluorescence spectroscopy provides information about the molecular environment in the vicinity of Tyr and Trp residues and has several advantages, such as sensitivity, spectral simplification, spectral bandwidth reduction, and the possibility to avoid various perturbing effects. Synchronous fluorescence spectra were obtained by scanning simultaneously the excitation and emission monochromators and only showed the Tyr residues and the Trp residues of HSA for wavelength intervals, $\Delta\lambda$, of respectively 15 and 60 nm.³¹

Figure 4 presents the original peaks for the system when $\Delta\lambda = 15$ and 60 nm. As we can see, an increase in ciprofloxacin concentration from 0 to $1.66 \times 10^{-3} \text{ mM}$ caused the fluorescence intensity to decrease in all systems. Moreover,

Table 5. Binding Parameters of HSA–Ciprofloxacin Complex at $\lambda_{\text{ex}} = 280 \text{ nm}$ in the Presence and Absence of Silver Nanoparticles

system	n_1	n_2	K_{a1}	K_{a2}	R_1	R_2
HSA–ciprofloxacin	1.26		1.95×10^3		0.991	
(HSA-AgI)–ciprofloxacin	0.53	1.30	5.01×10	2.01×10^4	0.998	0.989
(HSA-AgII)–ciprofloxacin	1.15	0.64	1.57×10^4	3.14×10^2	0.999	0.993
(HSA-AgIII)–ciprofloxacin	1.03		6.15×10^3		0.999	

Table 6. Binding Parameters of HSA–Ciprofloxacin Complex at $\lambda_{\text{ex}} = 295$ nm in the Presence and Absence of Silver Nanoparticles

system	n_1	n_2	$K_{\text{a}1}$	$K_{\text{a}2}$	R_1	R_2
HSA–ciprofloxacin	0.97		1.61×10^3		0.980	
(HSA-AgI)–ciprofloxacin	1.34	0.49	3.09×10^5	3.54×10	0.988	0.993
(HSA-AgII)–ciprofloxacin	0.93	0.64	2.3×10^3	2.65×10^2	0.981	0.996
(HSA-AgIII)–ciprofloxacin	0.79		8.0×10^2		0.980	

according to the figure, the synchronous fluorescence of HSA–ciprofloxacin and (HSA-nanosilver)–ciprofloxacin did not show any wavelength shift at $\Delta\lambda = 15$ or 60 nm. It was thus concluded that ciprofloxacin and silver nanoparticles did not affect the shift of the emission maximum of HSA in the binary and ternary systems at $\Delta\lambda = 15$ and 60 nm. In other words, no change in the polarities of the protein fluorophore environments occurred when the concentration of the drug was increased in the presence and absence of silver nanoparticles.

Figure 5A shows the slope of the plot of HSA–ciprofloxacin complex and Figure 5 panels B, C, and D present the slopes of the plots of (HSA-AgI)–ciprofloxacin, (HSA-AgII)–ciprofloxacin, and (HSA-AgIII)–ciprofloxacin complexes, respectively. In Figure 5A,C,D, the slope was higher when $\Delta\lambda$ was 60 nm, which led to the conclusion that Trp played an important role during fluorescence quenching of HSA. This signified that HSA approached the Trp more than the Tyr residues, but for the (HSA-AgI)–ciprofloxacin system displayed in Figure 5B, it was the other way around. Thus, a change in size of the silver nanoparticles modified the application and behavior of the complex.

3.5. Resonance Light Scattering. In recent years, the resonance light scattering (RLS) technique has gradually gained the interest of analytical chemists. It is characterized by high sensitivity, convenience in performance, and simplicity of the apparatus (usually a common spectrofluorometer). The RLS technique has been widely used on proteins and has also been successfully applied to biochemical, environmental, and food analyses. The RLS technique can be used to provide insight into the process responsible for the formation of a complex, which depends on its size and shape as well as on the index of refraction relative to the surrounding medium, and scattering. In total, an enhancement of light-scattering is dependent on (1) resonance-enhanced light scattering, (2) molecular polarizability, (3) enhancement of hydrophobicity, and (4) increase in molecular volume (or molecular weight).³² RLS is calculated according to the following formula:³³

$$I_{\text{RLS}} = (32\pi^3 V^2 n^2 N / \lambda^4) [(\delta n)^2 + (\delta k)^2] \quad (7)$$

where n is the refractive index of the medium, N is the molarity of the solution, λ is the wavelength of incident and scattered light, V is the square of the molecular volume, and δn and δk are the fluctuations in real and imaginary components of the refractive index of the particle, respectively.

When other factors are held constant, I_{RLS} is related to the size of the formed particle and is directly proportional to the square of the molecular volume. Therefore, with an increase in molecular volume, the RLS intensity of the system becomes greatly enhanced. The RLS technique is available to provide insight into the process responsible for the formation of a complex.³⁴

By scanning both the excitation and emission monochromators of a common spectrofluorometer with $\Delta\lambda = 0$ nm, RLS spectra can be recorded. The technique is able to investigate

the aggregation of small molecules and the long-range assembly of organic dyes on biological templates.³⁵ Figure 6 displays the curves of ΔI_{RLS} versus ciprofloxacin concentration, represented as $\Delta I_{\text{RLS}} = I_{\text{RLS}} - I_{0,\text{RLS}}$ (where I_{RLS} and $I_{0,\text{RLS}}$ are the RLS intensities of the systems with and without ligands, respectively). The RLS intensity of the ternary systems increased when the ciprofloxacin concentration was raised. The results showed that the critical induced aggregation concentration (C_{CIAC}) of ciprofloxacin was increased from 1×10^{-5} mM to 2×10^{-5} mM after the addition of silver nanoparticles. This phenomenon further proves that silver nanoparticles can induce ciprofloxacin aggregation on HSA and even form precipitates, but there were no significant differences between three sizes of silver nanoparticles with regard to C_{CIAC} . The arrows in Figure 6 show the C_{CIAC} of ciprofloxacin in the absence and presence of nanosilver of different sizes. In the presence of nanosilver, C_{CIAC} of ciprofloxacin increases, which shows precipitation of drug on HSA.

3.6. Polarizability. The other possible reason for RLS enhancement was an effect of polarizability on the scattering intensity. The light scattering formula derived by Stanton is written as follows:

$$I = (16\pi^2 P_N I_0 / \lambda^4 r^2) |\bar{\alpha}|^2 \quad (8)$$

where P_N is the number density of the molecules, I_0 is the intensity of incident light, λ is the incident wavelength, r is the distance from the molecule to the observer, and $\bar{\alpha}$ is the molecular polarizability (composed of a real and an imaginary part). It can be seen that the scattering intensity is directly proportional to the polarizability. A large increase in polarizability is thus one of several important factors for enhancement of RLS and formation of complexes.³⁶

The mean polarizability and energies of HSA and ciprofloxacin in the presence of silver nanoparticles were calculated at the B3LYP/LANL2MB theoretical level, and the values are listed in Table 7. By means of density functional theory (DFT), the structure of HSA and ciprofloxacin in the presence and absence of silver nanoparticles of three different sizes was optimized. As can be seen from Table 7, the mean polarizability of native HSA increased from 338.17 to 339.35, 339.74, and 339.81 in the presence of AgI, AgII, and AgIII, respectively. Also, an increase to 385.16 was observed when HSA was titrated with ciprofloxacin. The results show that the size of the silver nanoparticles influenced the mean polarizability; that is, when the size of the silver nanoparticles increased, the mean polarizability of (HSA-Ag)–ciprofloxacin also increased. These polarizability data confirmed the RLS results.

3.7. Red Edge Excitation Shift. Red edge excitation shift (REES) of fluorescence can be used as a parameter for studying the photophysical and chemical properties of isolated proteins. Fluorescence decay rates and wavelengths of maximum emission of a protein display dependence on the excitation wavelength if the protein matrix relaxes slowly around the

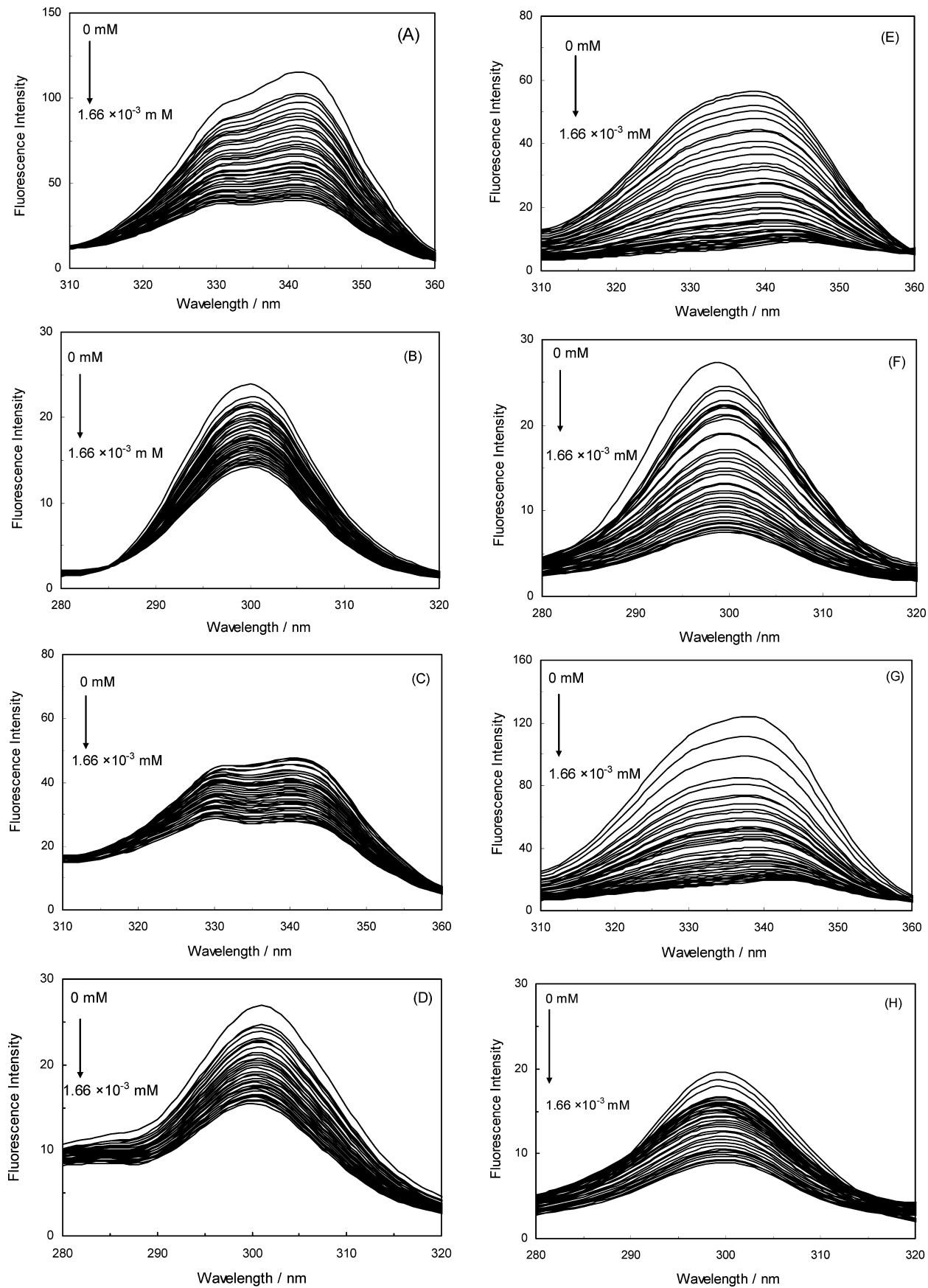


Figure 4. Synchronous fluorescence spectra of the binary system of HSA with various concentrations of (A, B) ciprofloxacin at $\Delta\lambda =$ (A) 60 nm and (B) 15 nm; (C, D) (HSA-AgI)-ciprofloxacin at $\Delta\lambda =$ (C) 60 nm and (D) 15 nm; (E, F) (HSA-AgII)-ciprofloxacin at $\Delta\lambda =$ (E) 60 nm and (F) 15 nm; and (G, H) (HSA-AgIII)-ciprofloxacin at $\Delta\lambda =$ (G) 60 nm and (H) 15 nm.

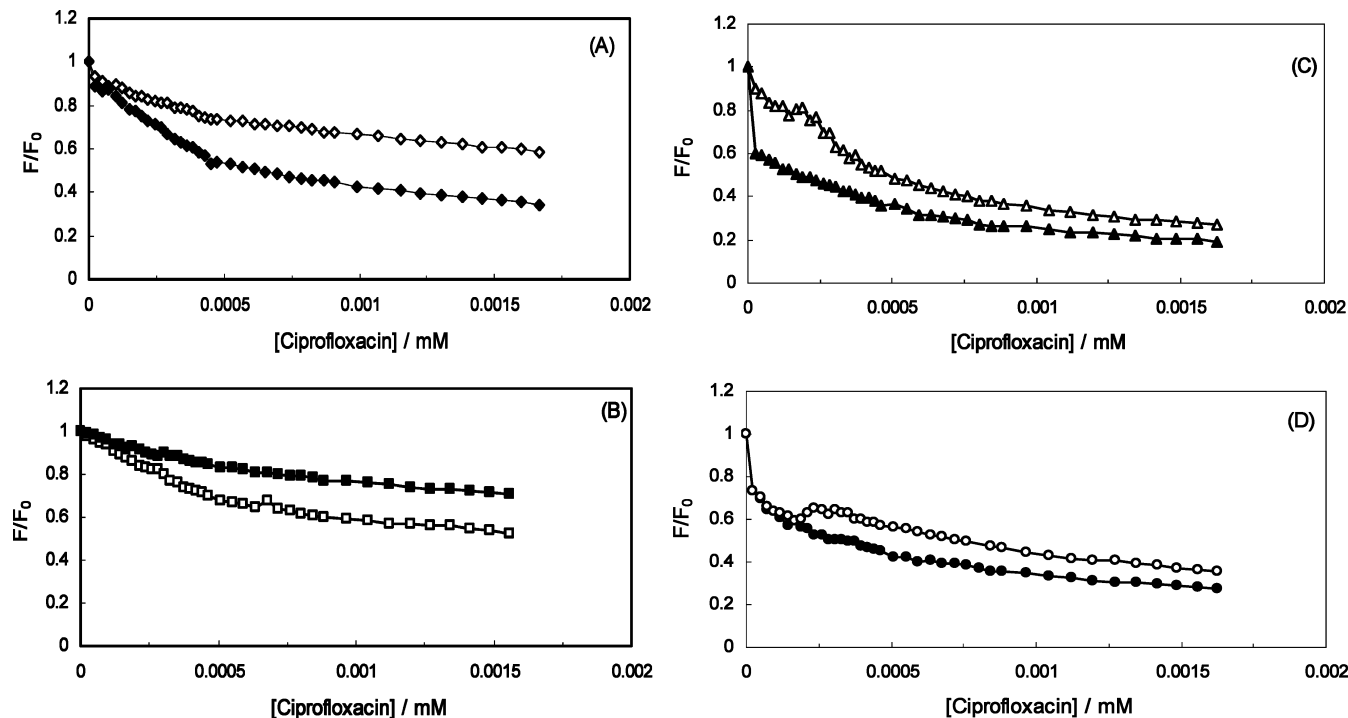


Figure 5. Quenching of synchronous fluorescence of (A) HSA–ciprofloxacin at $\Delta\lambda = (\blacklozenge)$ 60 nm and (\lozenge) 15 nm; (B) (HSA-AgI)–ciprofloxacin at $\Delta\lambda = (\blacksquare)$ 60 nm and (\square) 15 nm; (C) (HSA-AgII)–ciprofloxacin at $\Delta\lambda = (\blacktriangle)$ 60 nm and (\triangle) 15 nm; and (D) (HSA-AgIII)–ciprofloxacin at $\Delta\lambda = (\bullet)$ 60 nm and (\circ) 15 nm.

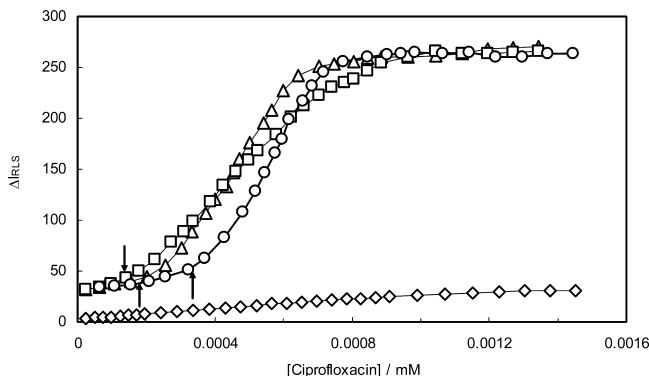


Figure 6. ΔI_{RLS} versus [ciprofloxacin] for (\diamond) HSA–ciprofloxacin, (\square) (HSA–AgI)–ciprofloxacin, (\triangle) (HSA–AgII)–ciprofloxacin, and (\circ) (HSA–AgIII)–ciprofloxacin.

Table 7. Calculated Effect of Polarizabilities and Energies of HSA and Ciprofloxacin in the Presence of Silver Nanoparticles

system	polarizability/au
HSA	338.17
HSA–ciprofloxacin	385.16
HSA-AgI	339.35
HSA-AgII	339.74
HSA-AgIII	339.81
(HSA-AgI)–ciprofloxacin	387.49
(HSA-AgII)–ciprofloxacin	390.13
(HSA-AgIII)–ciprofloxacin	390.79

increased dipole moment of the excited state.³⁷ Measurements of fluorescence emission and red edge excitation shift (REES) of HSA upon interaction with ciprofloxacin in the presence of

three different-sized silver nanoparticles rendered it possible to compare the environmental and mobility features of the Trp residue in HSA–drug complexes.

REES is a shift in the emission maximum toward a higher wavelength caused by a change in position in the excitation wavelength toward the red edge of the absorption band. It is caused by electronic coupling between Trp indole rings and neighboring dipoles and occurs when there are slow relaxations of solvent media. Thus, REES is particularly useful in monitoring motions around the Trp residues in protein studies.^{37,38}

The results of the REES investigation for the complexes in question are listed in Table 8. As can be seen, the value of REES for the HSA–ciprofloxacin system was 5, and in the

Table 8. Red Edge Excitation Shift Effects at $\lambda_{ex} = 305$ and 295 nm^a

system	ratio	max λ_{em}/nm		$\Delta\lambda$
		$\lambda_{ex} = 295 \text{ nm}$	$\lambda_{ex} = 305 \text{ nm}$	
HSA–ciprofloxacin	1:5	344	339	5
HSA–ciprofloxacin	1:10	344	339	5
(HSA-AgI)–ciprofloxacin	1:5	326	338	12
(HSA-AgI)–ciprofloxacin	1:10	326	338	12
(HSA-AgII)–ciprofloxacin	1:5	333	338	5
(HSA-AgII)–ciprofloxacin	1:10	332	339	7
(HSA-AgIII)–ciprofloxacin	1:5	331	339	8
(HSA-AgIII)–ciprofloxacin	1:10	332	338	6

^aExperiments were conducted at pH 7.4 and 298 K.

presence of the silver nanoparticles, the REES value was augmented. These data indicate that the presence of silver nanoparticles caused more rigidity in the Trp environment and

that there was more hydrogen bound around the Trp residue, reducing its mobility. Also, when the REES values for the different sizes of nanosilver were compared, we could conclude that each size gave rise to different behavior.

3.8. Three-Dimensional Fluorescence Spectroscopy.

Three-dimensional fluorescence spectroscopy has become a popular technique in recent years. The outstanding advantage of the method is that information on fluorescence characteristics can be entirely acquired by simultaneously changing excitation and emission wavelengths.³⁹ Excitation wavelength, emission wavelength, and fluorescence intensity can be used as the axes, making the investigation of the characteristic conformational changes of proteins more scientific and credible.⁴⁰

The three-dimensional spectra and contour maps of the HSA–ciprofloxacin complex are presented in Figure 7. According to the figure, peak a is the Rayleigh scattering

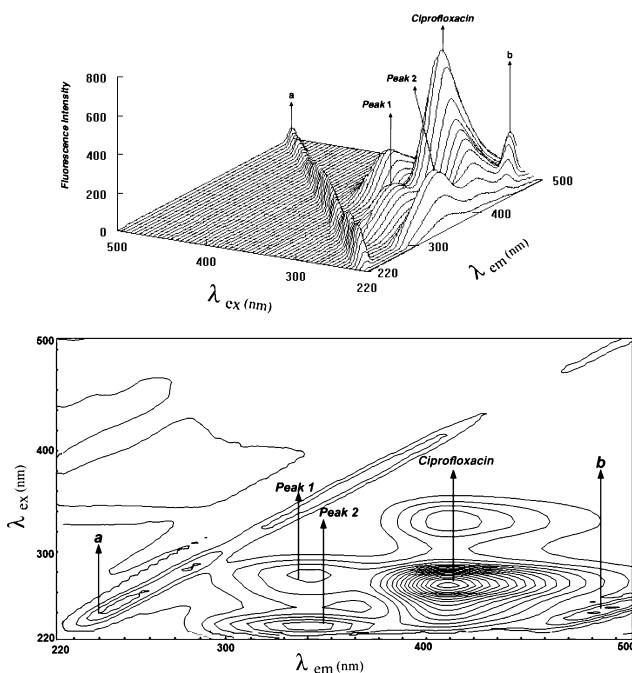


Figure 7. (A) Three-dimensional fluorescence and (B) contour map of the HSA–ciprofloxacin system. HSA and ciprofloxacin concentrations were 4.52×10^{-6} mM and 4.7×10^{-5} mM, respectively.

peak ($\lambda_{\text{ex}} = \lambda_{\text{em}}$), and peak b is the second-order scattering peak ($\lambda_{\text{ex}} = 2\lambda_{\text{em}}$), which is mainly caused by the $\pi \rightarrow \pi^*$ transition of the characteristic polypeptide backbone structure C=O of HSA.⁴⁸ Peak 1 ($\lambda_{\text{ex}} = 275$ nm, $\lambda_{\text{em}} = 345$ nm) is the fluorescence peak that primarily expresses the spectral behavior of the Tyr and Trp residues, since excitation of HSA at 280 nm reveals the intrinsic fluorescence of these moieties. The fluorescence of the Phe residue, on the other hand, is negligible.⁴¹

In comparison to peak 1, another fluorescence peak 2 ($\lambda_{\text{ex}} = 235$ nm, $\lambda_{\text{em}} = 344$ nm) had the characteristic polypeptide backbone structure of HSA.⁴² It was obvious that both fluorescence peaks a and b of HSA had been quenched by ciprofloxacin, albeit to different extents, as shown in Table 9. This was evidence of complex formation between ciprofloxacin and HSA, causing a change in the conformation of HSA. Moreover, the results indicated that the microenvironment had undergone significant alterations during formation of the

Table 9. Three-Dimensional Fluorescence Characteristics of HSA–Ciprofloxacin Complexes

system	peak 1 ($\lambda_{\text{ex}}/\lambda_{\text{em}}$)	$\Delta\lambda$	intensity	peak 2 ($\lambda_{\text{ex}}/\lambda_{\text{em}}$)	$\Delta\lambda$	intensity
HSA	270/344	74	934	235/344	109	717
HSA–ciprofloxacin	275/345	70	182	235/344	109	297
(HSA-AgI)–ciprofloxacin	280/338	58	139	235/336	101	192
(HSA-AgII)–ciprofloxacin	280/335	55	132	235/335	100	192
(HSA-AgIII)–ciprofloxacin	280/344	64	54	230/342	112	123

HSA–ciprofloxacin complex and that the structure of HSA had been modified by the binding of ciprofloxacin.⁴³

It can also be seen in Table 9 that λ_{ex} , λ_{em} and intensities of peaks 1 and 2 changed in different ways in the presence of the three sizes of silver nanoparticles. This indicated that each size of silver nanoparticles had its own special effect on the HSA–ciprofloxacin complex.

3.9. Energy Transfer between Ciprofloxacin and HSA.

Fluorescence resonance energy transfer (FRET) has been used as a “spectroscopic ruler” for measuring molecular distances in biological and macromolecular systems. According to Förster’s nonradiative energy transfer theory,^{44,45} energy transfer occurs under the following conditions: (1) when the donor can produce fluorescent light, (2) when the fluorescence emission spectrum of the donor and UV absorbance spectrum of the acceptor overlap, and (3) when the distance of approach between donor and acceptor is lower than 7 nm. The energy transfer effect is related not only to the distance between acceptor and donor (r_0) but also to the critical energy transfer distance (R_0), according to

$$E = 1 - \frac{F}{F_0} = \frac{R_0^6}{R_0^6 + r^6} \quad (9)$$

Here F and F_0 are the fluorescence intensities of HSA in the presence and absence of ciprofloxacin, respectively; r is the distance between the acceptor and donor; and R_0 is the critical distance when the transfer efficiency is 50%.

$$R_0^6 = (8.79 \times 10^{-25}) K^2 n^{-4} \emptyset J \quad (10)$$

where K^2 is the spatial orientation factor of the dipole, n is the refractive index of the medium, \emptyset is the fluorescence quantum yield of the donor, and J is the overlap integral of the fluorescence emission spectrum of the donor and the absorption spectrum of the acceptor. The latter can be calculated by

$$J = \left[\sum F(\lambda) \varepsilon(\lambda) \lambda^4 \Delta\lambda \right] / \sum F(\lambda) \Delta\lambda \quad (11)$$

where $F(\lambda)$ is the fluorescence intensity of the fluorescence donor at wavelength λ and $\varepsilon(\lambda)$ is the molar absorption coefficient of the acceptor at wavelength λ .⁴⁶

The overlap integral J could be evaluated by investigating the spectra in Figure 8. The parameters regarding FRET are presented in Table 10. The average distance $r < 8$ nm and $0.5R_0 < r < 1.5R_0$, which implied that the energy transfer from HSA to ciprofloxacin occurred with a high probability. Moreover, the results in Table 8 suggest that the distance between bound drug and HSA differed in the presence of the three different sizes of

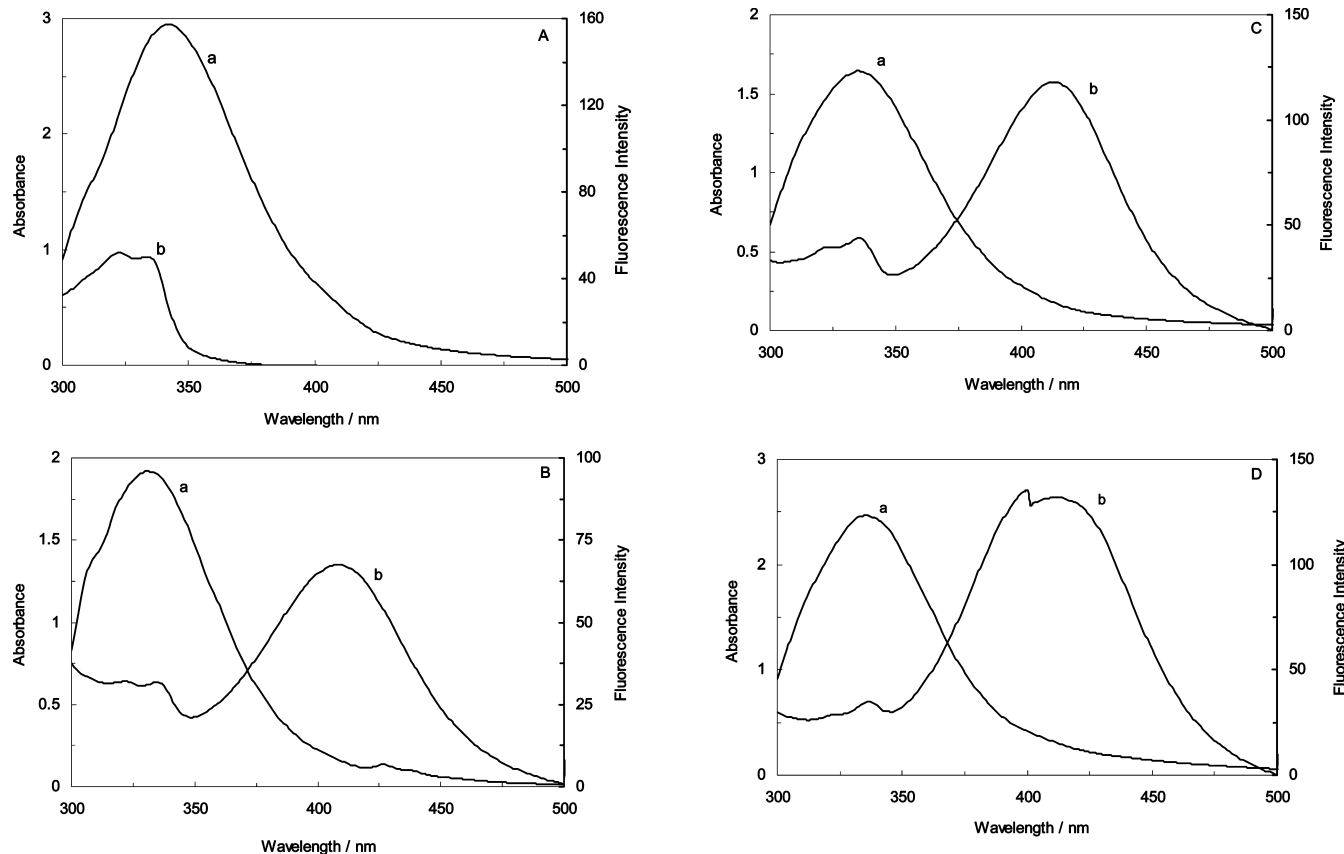


Figure 8. Overlap of fluorescence emission (curve a) of HSA with absorption spectra (curve b) of (A) ciprofloxacin, (B) ciprofloxacin-AgI, (C) ciprofloxacin-AgII, and (D) ciprofloxacin-AgIII; $T = 298\text{ K}$, pH 7.4, $C_{[\text{HSA}]} = C_{[\text{ciprofloxacin}]} = 4.52 \times 10^{-6}\text{ mM}$, and the concentration of nanosilver was $1.4 \times 10^{-3}\text{ mM}$.

Table 10. Distance between Donor and Acceptor of HSA with Ciprofloxacin and Silver Nanoparticles as Binary and Ternary Systems^a

system	r/nm
HSA–ciprofloxacin	2.46
(HSA-AgI)–ciprofloxacin	1.73
(HSA-AgII)–ciprofloxacin	1.89
(HSA-AgIII)–ciprofloxacin	2.13

^aExperiments were performed at pH 7.4 and 298 K.

silver nanoparticles. It was clear that nanosilver size III gave rise to a higher affinity in the HSA binding to ciprofloxacin than the other nanoparticles, but the distance between ciprofloxacin and HSA in this system was larger than in the others. This was due to long-range effects of nanosilver size III.

3.10. Circular Dichroism and Conformational Analysis. The circular dichroism (CD) technique was used to further verify the interaction between ciprofloxacin and HSA. To clearly understand how the structure of HSA was affected by the drug, CD measurements were first performed on free HSA (Figure 9). The data are expressed as molar residue ellipticity $[\theta]$, defined as $[\theta] = 100\theta_{\text{obs}}/c$, where θ_{obs} is the observed ellipticity in degrees and c is the concentration, when the other parameters are constant, that is, 4 s, a 2-nm bandwidth, a scan rate of $5\text{ nm}\cdot\text{min}^{-1}$, and a 1-mm path length cell from 250 to 190 nm. The thus-determined CD for α -helix, β -sheet and random forms can be conversely used to estimate the secondary structure of any protein with X at several

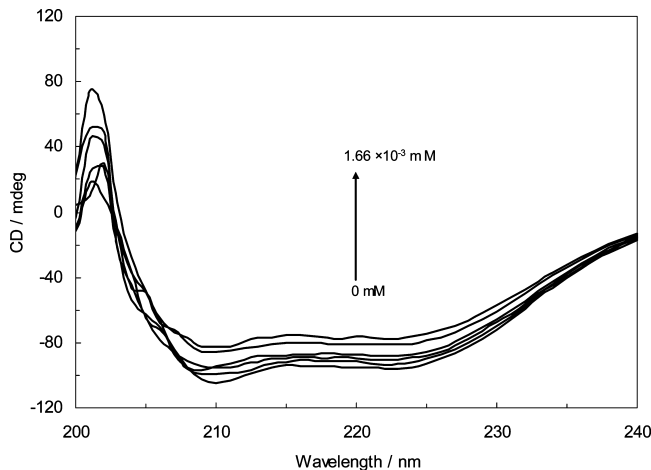


Figure 9. Far-UV CD spectra of free HSA in the presence of various concentrations of ciprofloxacin. Conditions: $T = 298\text{ K}$, pH = 7.4, $[HSA] = 0.01\text{ w/v}$, $[ciprofloxacin] = 0$ to $1.66 \times 10^{-3}\text{ mM}$.

wavelengths for the same equation. The α -helical content (f_H) was estimated from the ellipticity value at 222 nm ($[\theta]_{222}$) according to^{47,48}

$$f_H = -(([\theta]_{222} + 2340)/30300) \quad (12)$$

Table 11 lists the secondary structural elements that were calculated. The acquired data suggest that the secondary structure of free HSA consisted of 53.97% α -helix, 18.31% β -sheet, 13.48% turn, and 14.25% unordered coil. The results in

Table 11. Secondary Structure Content of HSA upon Interaction with Ciprofloxacin in the Presence of Silver Nanoparticles

system	α -helix, %	β -sheet, %	turn, %	unordered coil, %
HSA	53.97	18.31	13.48	14.25
HSA–ciprofloxacin	50.27	17.05	13.14	19.54
(HSA-AgI)–ciprofloxacin	48.62	16.27	12.37	22.74
(HSA-AgII)–ciprofloxacin	49.17	16.73	13.05	21.05
(HSA-AgIII)–ciprofloxacin	49.91	16.88	13.11	20.1

Table 11 show that the percentage of α -helix decreased gradually, from 53.97% in free HSA to 50.27% upon ciprofloxacin binding indicating a certain degree of destabilization. Similar results were observed upon the binding of ciprofloxacin to HSA-nanosilver systems in ternary complexes, as shown in Table 11.

From these results, it was apparent that binding of ciprofloxacin to HSA caused a conformational change of the protein, with a loss of α -helix stability. Furthermore, it can be concluded that occupancy of the Trp sites by the binding ligands could actually stabilize the native conformation of the protein. When the three different sizes of silver nanoparticles were compared, the biggest size had the least effect on the secondary structure of HSA, whereas nanosilver size I had the most significant influence on HSA's secondary structure.

3.11. Zeta Potential. Each particle dispersed in a solution is surrounded by oppositely charged ions called the fixed layer. Outside the fixed layer, there are varying compositions of ions of opposite polarities, forming a cloudlike area—called the diffuse double layer—that is electrically neutral. When a voltage is applied to the solution in which particles are dispersed, these are attracted to the electrode of the opposite polarity, accompanied by the fixed layer and part of the diffuse double layer, or the internal side of the “sliding surface”. The ζ potential is considered to be the electric potential of this inner area including this conceptual “sliding surface”. As this electric potential approaches zero, particles tend to aggregate.⁴⁹ In order to confirm the existence of drug binding, ζ potential measurements were carried out at physiological pH.⁵⁰

The ζ potential was calculated from the electrophoretic mobilities, μ_E , by use of the Henry equation:

$$Z = (3\mu E \eta / 2\epsilon_0 \epsilon_r)[1/f(ka)] \quad (13)$$

where ϵ_0 is the permittivity of vacuum; ϵ_r and η are the relative permittivity and viscosity of water, respectively; a is the particle radius; and k is the Debye length. The function $f(ka)$ depends on the particle shape, and for our systems it was determined by

$$f(ka) = \frac{2}{3} - \frac{9}{2ka} + \frac{75}{2k^2 a^2} - \frac{330}{k^3 a^3} \quad (14)$$

and was valid for $ka > 1$.⁵¹

As illustrated in Figure 10, the ζ potential value of native HSA in the absence of ciprofloxacin was -6.16 mV. Upon addition of ciprofloxacin to HSA, the ζ potential increased, which indicated the formation of an HSA–ciprofloxacin complex. Up to a ciprofloxacin concentration of 1.2×10^{-4} mM, electrostatic interactions are the main forces between HSA and ciprofloxacin, but at higher amounts, the hydrophobic interactions became predominant. Consequently, the inflection point for this system was 1.2×10^{-4} mM.

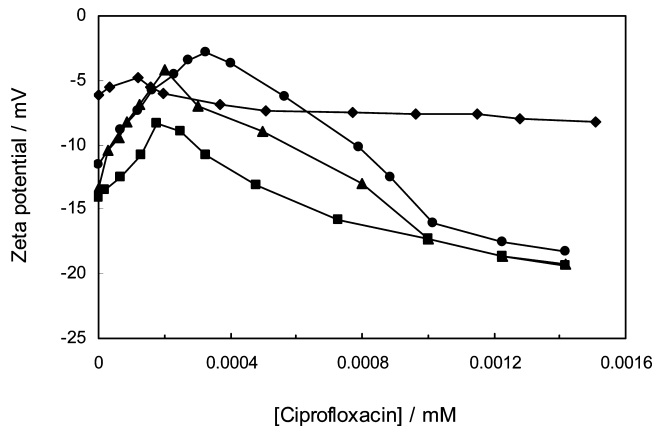


Figure 10. Zeta potential of HSA as a function of ciprofloxacin concentration: (◊) HSA–ciprofloxacin, (□) (HSA-AgI)–ciprofloxacin, (△) (HSA-AgII)–ciprofloxacin, and (○) (HSA-AgIII)–ciprofloxacin.

In the presence of silver nanoparticles, the electrostatic interactions were greater than in the binary system, and the inflection point changed to 1.7×10^{-4} mM for (HSA-AgI)–ciprofloxacin, 2×10^{-4} mM for (HSA-AgII)–ciprofloxacin, and 3×10^{-4} mM for (HSA-AgIII)–ciprofloxacin. These data testify to the electrostatic interactions being more significant in the HSA–ciprofloxacin complex in the presence of silver nanoparticles.

Figure 11 displays the polydispersity index (PDI) of the HSA–ciprofloxacin complex in the presence and absence of three different sizes of silver nanoparticles. The polydispersion index is a parameter between 1 and 0 portraying the dispersion

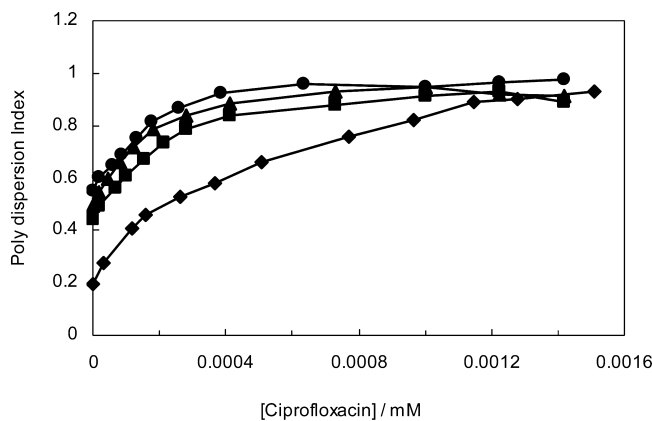


Figure 11. Dependence of the polydispersity index of HSA on ciprofloxacin concentration in the presence and absence of silver nanoparticles: (◊) HSA–ciprofloxacin, (□) (HSA-AgI)–ciprofloxacin, (△) (HSA-AgII)–ciprofloxacin, and (○) (HSA-AgIII)–ciprofloxacin.

in a sample. The PDI can be used for values greater than 0.1, and between 0.1 and 0.2 it represents a narrow particle size distribution.⁵²

The PDI value for native HSA was 0.2, and it increased when silver nanoparticles were added (data not shown). Also, as can be seen from Figure 11, this value increased when HSA was titrated by ciprofloxacin. In our study, the PDI values for ternary systems were higher than in the binary complexes, signifying that the presence of silver nanoparticles caused increased dispersion in the system. When the PDI values for the

ternary systems are compared, we can conclude that the different-sized silver nanoparticles induced different effects on the PDI of the HSA–ciprofloxacin complex.

CONCLUSION

The interaction between ciprofloxacin and HSA in the presence and absence of silver nanoparticles of three different sizes was compared by various spectroscopic and ζ potential methods. It was shown that the binding affinity of ciprofloxacin to HSA in the presence of silver nanoparticles was higher than in their absence. Also, with increasing size of the nanosilver, the binding affinity was raised.

The binding of ciprofloxacin to HSA caused a blue shift in the fluorescence spectra that corresponded to decreased polarity of the microenvironment. The quenching curves indicated that ciprofloxacin bound to both the Trp and Tyr residues of HSA via a static quenching mechanism. In the ternary systems, there were some changes in the quenching mechanism in the presence of silver nanoparticles of size I and II; that is, there occurred two kinds of static quenching mechanism with two different binding sites.

RLS results indicated that the critical concentration of the HSA–ciprofloxacin system decreased in the presence of silver nanoparticles. Binding of ciprofloxacin to HSA induced structural changes in the conformation of the protein and a decrease in α -helix percentage. However, with an increase in silver nanoparticle size in the ternary systems, the secondary structure of HSA was more established. On the basis of ζ potential data, we could conclude that the critical aggregation concentration of ciprofloxacin was altered by changes in the hydrophobic interactions due to the presence of silver nanoparticles.

AUTHOR INFORMATION

Corresponding Author

*Telephone + 98511 8437107; fax + 98511 8424020; e-mail chamani@ibb.ut.ac.ir or chamani_J@yahoo.com.

ACKNOWLEDGMENTS

The Research Council of the Mashhad Branch, Islamic Azad University, Mashhad, Iran, is gratefully acknowledged for financial support. We thank Dr. Ljungberg for the English editing.

REFERENCES

- (1) Ghali, M.; Kummel, T.; Bacher, G.; Wenisch, J.; Brunner, K. *Appl. Phys. Lett.* **2008**, *93*, 73–107.
- (2) Wang, Y.; Tang, Z.; Kotov, N. A. *Mater. Today* **2005**, *8* (5), 20–31.
- (3) Ghali, M. *J. Lumin.* **2010**, *130*, 1254–1257.
- (4) Hardman, R. *Environ. Health Perspect.* **2006**, *116*, 165–174.
- (5) Chen, X.; Schluesener, H. *J. Toxicol. Lett.* **2008**, *176*, 1–12.
- (6) Cai, W.; Fan, Y.; Jiang, Z.; Yao, J. *Talanta* **2010**, *81*, 1810–1815.
- (7) Choi, O.; Yu, C.; Fernandez, G. E.; Hu, Z. *Water Res.* **2010**, *44*, 6095–6103.
- (8) Seedher, N.; Agarwal, P. *J. Lumin.* **2010**, *130*, 1841–1848.
- (9) Zakelj, S.; Sturm, K.; Kristl, K. *Int. J. Pharm.* **2006**, *313*, 175–180.
- (10) Breilh, D.; Saux, M. C.; Maire, P.; Vergnaud, J. M.; Jelliffe, R. W. *Comput. Biol. Med.* **2001**, *31*, 147–155.
- (11) Periti, P.; Mazzei, T.; Curti, M. E.; et al. *Int. J. Antimicrob. Agent.* **1998**, *10*, 215–222.
- (12) Cater, D. C.; Ho, J. X. *Adv. Protein Chem.* **1994**, *45*, 153–203.
- (13) Peters, T. *Adv. Protein Chem.* **1985**, *37*, 161–170.
- (14) Curry, S.; Brich, P.; Frank, N. P. *Biochem. Biophys. Acta.* **1999**, *14*, 41–131.
- (15) Tang, K.; Qin, Y. M.; Lin, A. H.; Hu, X.; Zou, G. L. *J. Pharm. Biomed. Anal.* **2005**, *39*, 404–410.
- (16) Tang, J.; Lian, N.; He, X.; Zhang, G. *J. Mol. Struct.* **2008**, *889*, 408–414.
- (17) Bourassa, P.; Kanakis, C. D.; Tarantilis, P.; Polissiov, M. G.; Tajmir-Riahi, H. A. *J. Phys. Chem. B* **2010**, *114*, 3348–3354.
- (18) Bourassa, P.; Dubeau, S.; Maharvi, G. M.; Fauq, A. H.; Thomas, T. J.; Tajmir-Riahi, H. A. *Biochimie* **2011**, *93*, 1089–1101.
- (19) Li, Y.; He, W. Y.; Liu, H.; Yao, X.; Hu, Z. *J. Mol. Struct.* **2007**, *83*, 144–150.
- (20) Froehlich, E.; Mandeville, J. S.; Kreplak, L.; Tajmir-Riahi, H. A. *Biomacromolecules* **2011**, *12*, 2780–2787.
- (21) Qi, Z.; Zhang, Y.; Liao, F.; Qu_Yang, Y. W.; Liu, Y.; Yang, X. *J. Pharm. Biomed. Anal.* **2008**, *46*, 699–706.
- (22) Vaidyanathan, R.; Kalishwaralal, K.; Gopalram, S.; Gurunathan, S. *Biotechnol. Adv.* **2009**, *27*, 924–937.
- (23) Wei, Y.; Li, J.; Dong, C.; Shung, S.; Liu, D.; Huie, C. W. *Talanta* **2006**, *70*, 377–382.
- (24) Zhang, H.-M.; Wang, Y.-Q.; Jiang, M.-L. *Dyes Pigm.* **2009**, *82*, 156–163.
- (25) Sulkowska, A. *J. Mol. Struct.* **2002**, *614*, 227–232.
- (26) Chamani, J.; Tafrishi, N.; Momen-Heravi, M. *J. Lumin.* **2010**, *130*, 1160–1168.
- (27) Chopra, A. *J. Antimicrob. Chemother.* **2007**, *59*, 587–90.
- (28) Hu, Y.; Wang, Y.; Ou-Yang, Y.; Zhou, J.; Liu, Y. *J. Lumin.* **2010**, *130*, 1394–1399.
- (29) Wei, X. L.; Xiao, J. B.; Wang, Y.; Bai, Y. *Spectrochim. Acta, Part A* **2010**, *75*, 299–304.
- (30) Lloyd, J.; Evett, W. *Anal. Chem.* **1997**, *49*, 1710–1715.
- (31) Wang, Y. P.; Wei, Y. L.; Dong, C. *J. Photochem. Photobiol. A* **2006**, *177*, 6–11.
- (32) Meynier, C.; Guerlesquin, F.; Roche, P. *J. Biomol. Struct. Dyn.* **2009**, *27*, 49–57.
- (33) Huang, H. J.; Lee, K. J.; Yu, H. W.; Chen, H. Y.; Tsai, F. J.; Chen, C. Y. C. *J. Biomol. Struct. Dyn.* **2010**, *28*, 187–200.
- (34) Vahedian-Movahed, H.; Saberi, M. R.; Chamani, J. *J. Biomol. Struct. Dyn.* **2011**, *28*, 483–502.
- (35) Berman, H. M. *Acta. Crystallogr. A* **2008**, *64*, 88–95.
- (36) Sarzehi, S.; Chamani, J. *J. Biol. Macromol.* **2010**, *47*, 558–569.
- (37) ChenchalRao, S.; Mohan-Rao, C. H. *FEBS Lett.* **1994**, *337*, 269–273.
- (38) Demchenko, A. P. *J. Lumin.* **2002**, *17*, 2–19.
- (39) Rodríguez-Cuesta, M. J.; Boque, R.; Rius, F. X.; Zamora, D. P.; Galera, M. M.; Frenich, A. G. *Anal. Chim. Acta* **2003**, *491*, 47–56.
- (40) He, L.; Wang, X.; Lin, B.; Wang, J.; Sun, Y.; Gao, E.; Xu, S. *J. Lumin.* **2011**, *131*, 285–290.
- (41) Lakowicz, J. R. *Principles of Fluorescence Spectroscopy*; Springer Science + Business Media: New York, 2006.
- (42) Ding, F.; Liu, W.; Li, Y.; Zhang, L.; Sun, Y. *J. Lumin.* **2010**, *130*, 2–13.
- (43) Zhang, G.; Que, Q.; Pan, J.; Guo, J. *J. Mol. Struct.* **2008**, *881*, 132–138.
- (44) Lakowicz, J. R. *Principles of Fluorescence Spectroscopy*; Plenum Press: New York, 1983.
- (45) Sklav, L. A.; Hudson, B. S.; Simoni, R. D. *Biochemistry* **1977**, *16*, 5100–5108.
- (46) Chen, Z.; Liu, J.; Han, Y. *Talanta* **2007**, *71*, 12–46.
- (47) Hamed-Akbari, S.; Saberi, M. R.; Chamani, J. *Protein Pept. Lett.* **2010**, *17*, 1524–1535.
- (48) Chen, Y. H.; Yang, J. T.; Martinez, H. M. *Biochemistry* **1972**, *11*, 4120–4131.
- (49) Chamani, J. *J. Colloid Interface Sci.* **2006**, *299*, 636–646.
- (50) Omidvar, Z.; Parivar, K.; Sanee, H.; Amiri-Tehranzadeh, Z.; Baratian, A.; Saberi, M. R.; Asoodeh, A.; Chamani, J. *J. Biomol. Struct. Dyn.* **2011**, *29*, 181–206.
- (51) Amani, N.; Saberi, M. R.; Chamani, J. *Protein Pept. Lett.* **2011**, *18*, 935–951.

(52) Tantra, R.; Schulze, Ph.; Quincey, P. *Particuology* **2010**, *8*, 279–285.